Journal of Power Sources 222 (2013) 542–553

Contents lists available at SciVerse ScienceDirect

Journal of Power Sources

journal homepage: www.elsevier.com/locate/jpowsour

A comparison on effects of CO_2 on $La_{0.8}Sr_{0.2}MnO_{3+\delta}$ and $La_{0.6}Sr_{0.4}CoO_{3-\delta}$ cathodes

Zhe Zhao [a,b,c], Li Liu [a,b,c], Xiaomin Zhang [a,b,c], Weiming Wu [a,b,c], Baofeng Tu [a,b], Dingrong Ou [a,b], Mojie Cheng [a,b,*]

[a] Division of Fuel Cells, Dalian National Laboratory for Clean Energy, PR China
[b] Dalian Institute of Chemical Physics, Chinese Academy of Sciences, 457 Zhongshan Road, Dalian, Liaoning 116023, PR China
[c] Graduate University of the Chinese Academy of Sciences, Beijing 100039, PR China

HIGHLIGHTS

- Effects of carbon dioxide on performances and EIS of $La_{0.6}Sr_{0.4}CoO_{3-\delta}$ (LSC) cathode.
- Effects of carbon dioxide on performances and EIS of $La_{0.8}Sr_{0.2}MnO_{3-\delta}$ (LSM) cathode.
- CO_2 adsorption model on LSC from 550 °C to 800 °C.
- CO_2 adsorption model on LSM from 650 °C to 800 °C.

GRAPHICAL ABSTRACT

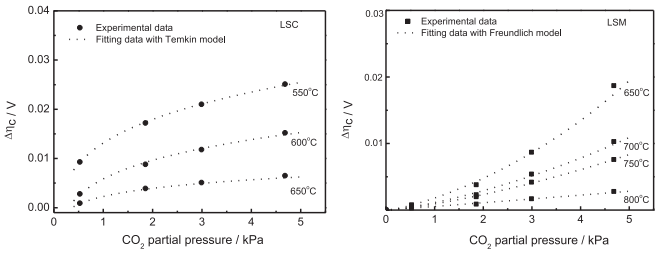

ARTICLE INFO

Article history:
Received 29 June 2012
Received in revised form
9 August 2012
Accepted 9 September 2012
Available online 14 September 2012

Keywords:
Solid oxide fuel cell
Carbon dioxide
Perovskite
Cathode
Adsorption model

ABSTRACT

The effects and affecting mechanisms of carbon dioxide on oxygen reduction reactions on the $La_{0.6}Sr_{0.4}CoO_{3-\delta}$ (LSC) and $La_{0.8}Sr_{0.2}MnO_{3+\delta}$ (LSM) cathodes have been investigated. The presence of CO_2 in O_2 flow reduces the LSC and LSM cell performance and increases polarization resistance. CO_2 impedes oxygen dissociative adsorption on the LSC cathode, whereas CO_2 inhibits dissociation of adsorbed oxygen molecule or diffusion of O-species on the LSM cathode. CO_2 adsorption on the LSC cathode obeys Temkin model in 550–650 °C and Freundlich model in 700–800 °C. Different CO_2 adsorption behaviors are ascribed to the change in LSC structure and the change in oxygen reduction mechanism. CO_2 adsorption on the LSM cathode obeys Freundlich model in 650–800 °C. The differences in the effects and affecting mechanisms of CO_2 on LSM and LSC are related to their differences in composition and structure.

1. Introduction

Sr-doped $LaMnO_3$ (LSM) and Sr-doped $LaCoO_3$ (LSC) are two of the most common materials used as cathodes in solid oxide fuel cells (SOFCs). LSM is the state-of-the-art cathode material for high-temperature SOFCs, mainly due to its high electronic conductivity, good stability with YSZ electrolyte and high electrochemical activity for oxygen reduction at high temperatures [1,2]. LSM usually displays oxygen excess nonstoichiometry due to the presence of stable Mn^{4+} ions [3,4]. Oxygen reduction on LSM takes place around the TPB and involves adsorption of oxygen molecule, dissociation of oxygen molecule, diffusion of oxygen atom, ionization of oxygen atom and incorporation of oxygen ion into electrolyte at TPB [5–10]. LSC is one of the most promising cathode materials for intermediate-and low-temperature SOFCs, mainly due to its high mixed ion–electron conductivity (MIEC) and high catalytic activity for oxygen reduction [11,12]. LSC displays oxygen deficient nonstoichiometry because of the difficulty in stabilizing

* Corresponding author. Dalian Institute of Chemical Physics, Chinese Academy of Sciences, 457 Zhongshan Road, Dalian, Liaoning 116023, PR China. Tel./fax: +86 411 84379049.
E-mail address: mjcheng@dicp.ac.cn (M. Cheng).

0378-7753/$ – see front matter © 2012 Elsevier B.V. All rights reserved.
http://dx.doi.org/10.1016/j.jpowsour.2012.09.023

Co^{4+} ions and ease of reduction of Co^{3+} to Co^{2+} [13]. Oxygen reduction on LSC extends to the whole cathode and involves oxygen dissociative adsorption, ionization of oxygen atom, diffusion of oxygen ion through LSC and transfer of oxygen ion from LSC bulk into the electrolyte [5,14–18]. Oxygen reduction reaction on perovskite cathode greatly depends on B-site cation and oxygen vacancy. B-site cations in perovskites are present in the form of B^{4+}/B^{3+} or B^{3+}/B^{2+} couples, which not only act as hopping sites for electrons/holes but also active sites for oxygen reduction. Oxygen vacancy is a predictor of oxygen ion bulk diffusion and oxygen surface reaction. The higher the amount of oxygen vacancies is available, the easier oxygen surface reaction is expected. But up to now, it is very difficult to clearly clarify oxygen reduction processes because reaction mechanism changes with material, composition, morphology and operating conditions [6,19,20].

Oxygen reduction can be hindered or blocked by some minor gases in air, such as SO_2, CO_2 and water vapor. Recently, the effects of these impurity gases on oxygen reduction reaction (ORR) on cathodes have been investigated [20–34]. The presence of CO_2 in oxygen flow seriously degrades the performance of BSCF cathode. The electrochemical impedance spectra (EIS) results show that the adsorbed CO_2 molecules occupy active sites for oxygen reduction especially at low temperatures [32]. The effects of CO_2 on oxygen reduction arise from the interaction of CO_2 with perovskite oxides. CO_2 adsorption on perovskite oxides $LaBO_3$ (B = Cr, Mn, Fe, Co, Ni) has been investigated using CO_2 temperature-programmed desorption (CO_2-TPD) and infrared spectroscopy [35–39]. The chemical nature of the B cation influences greatly the coverage of CO_2. Both monodentate carbonates and bidentate carbonates are formed on perovskite surfaces. Monodentate carbonates, bonding through C atom of CO_2 with basic O^{2-} ion, are facile to desorb at low temperature. Bidentate carbonates, bonding through C atom of CO_2 with O^{2-} ion in perovskite and O atom of CO_2 bonding with oxygen vacancy in perovskite, are relative stable. These different carbonate species may have different effects on oxygen reduction.

As a minor gas, it is impossible to completely remove CO_2 from air for SOFC practical applications. Therefore, it is important to know the effects and affecting mechanisms of CO_2 on oxygen reduction reactions on LSC and LSM cathodes. In this paper, we will investigate the effects of CO_2 on LSC and LSM cathodes and discuss the affecting mechanisms of CO_2 on oxygen reduction. The change of cathodic overpotential with CO_2 partial pressure is analyzed with different adsorption models on the two cathodes. The differences in the effects and affecting mechanisms of CO_2 on LSM and LSC cathodes are discussed in view of their composition and structural differences.

2. Experimental

Perovskite-type oxides $La_{0.6}Sr_{0.4}CoO_{3-\delta}$ (LSC) and $La_{0.8}Sr_{0.2}MnO_{3+\delta}$ (LSM) were prepared by the citric acid ammonium assisted Pechini-type method. Metal nitrates of La(NO_3)$_3$.6H_2O, Sr(NO_3)$_2$, Co(NO_3)$_2$.6H_2O and Mn(NO_3)$_2$ solution (50 wt %) were used as the raw materials. Metal nitrates at the stoichiometric ratios for the desired products were added into deionized water under stirring until a transparent solution was obtained. Then citric acid ammonium was added into the solution under stirring with a molar ratio of citric acid ammonium to total metal ions of 1.5. Water was evaporated at 90 °C until a transparent sol was formed. The primary powders were obtained from spontaneous combustion of the sols under heating. The grinded primary powders were subsequently calcined at 1000 °C for LSC and 1100 °C for LSM in a muffle in air.

The absolute oxygen content ($3 \pm \delta$) of synthesized $La_{0.6}Sr_{0.4}CoO_{3-\delta}$ (LSC) and $La_{0.8}Sr_{0.2}MnO_{3+\delta}$ (LSM) was measured through the decomposition of perovskite in a gas mixture of 10% H_2/Ar at 950 °C. Under the reduction condition, LSM decomposed to MnO, SrO and La_2O_3, and LSC decomposed to SrO, La_2O_3 and Co (metallic). The absolute oxygen content ($3 \pm \delta$) was calculated on the basis of the H_2 consumption monitored by a thermal conductivity detector (TCD). The absolute oxygen contents ($3 \pm \delta$) of initial $La_{0.6}Sr_{0.4}CoO_{3-\delta}$ (LSC) and $La_{0.8}Sr_{0.2}MnO_{3+\delta}$ (LSM) are 2.896 and 3.056, respectively.

The assemblies of anode NiO–YSZ supported with thin film of yttria-stabilized zirconia (YSZ) electrolyte (20 μm) were prepared by the tape-casting method. For the LSM cell, the composite cathode of LSM/YSZ was sintered at 1200 °C. A pure LSM layer onto the composite cathode was sintered at 1200 °C as a current collector layer. For the LSC cell, a barrier layer of ceria doped with Gd-cations (GDC) was deposited on the YSZ film through sputtering method. Pure LSC cathode was coated onto the GDC layer and sintered at 1050 °C. The active area of cathode was ca. 0.5 cm^2. The SEM photographs of the two cathodes were taken on a FEI QUANTA 200F microscope equipped with a field emission gun at 15 kV.

Humidified H_2 (3% H_2O) and pure O_2 flow were supplied as fuel and oxidant respectively. In order to investigate the effect of CO_2, CO_2 flow was blended into O_2 flow and fed to cathode. CO_2 partial pressure was controlled at 0.53, 1.85, 2.99 and 4.68 kPa in oxygen, respectively. The variations in cell voltage at constant current density of 0.15 A cm^{-2} were recorded after introducing O_2 flow with CO_2 for 10 min. The impedance spectra were typically measured under open circuit voltage conditions using a Solartron 1287 potentiostat and a 1260 frequency response analyzer. Scan parameters were as follows: frequency range of 0.08 Hz–98,500 Hz, 10 mV amplitude.

3. Results and discussion

Fig. 1 presents the surface and cross sectional SEM images of LSC and LSM cathodes. The particle size of LSC is in the range of 250–500 nm. The particle size of LSM is in the range of 1–2 μm. Both LSC and LSM cathodes show a structure with suitable porosity and well necked particles, which are prerequisites for gas diffusion and transfer of electron and/or oxygen ion.

Fig. 2 shows the current density–voltage curves of the LSC cell under different cathodic gas compositions. It can be seen that the cell performance decreases with increasing CO_2 partial pressure (P_{CO2}). At 0.7 V and 600 °C, the cell power density decreases by 1.81, 3.93, 5.05 and 7.15% at P_{CO2} = 0.53, 1.85, 2.99 and 4.68 kPa in oxidant. The corresponding area-specific resistance (ASR) calculated from current density–voltage curves increases by 0.02, 0.04, 0.06 and 0.09 Ω cm^2. The effect of CO_2 becomes serious with decreasing temperature. At P_{CO2} = 1.85 kPa, the cell power density at 0.7 V decreases by 0.45, 1.87 and 3.93% at 800, 700 and 600 °C, respectively. Fig. 3 shows the current density–voltage curves of the LSM cell under different cathodic gas compositions. The LSM cell performance decreases with increasing CO_2 partial pressure. At 0.7 V and 700 °C, the cell power density decreases by 0.76, 1.52, 4.05 and 6.47% at P_{CO2} = 0.53, 1.85, 2.99 and 4.68 kPa in oxidant. The corresponding area-specific resistance increases by 0.01, 0.03, 0.08 and 0.12 Ω cm^2.

Fig. 4 shows, in the form of Nyquist (Fig. 4a) and Bode (Fig. 4b) plots, the electrochemical impedance spectra of the LSC cell. The change of impedance spectra with CO_2 partial pressure is severer at low temperatures than that at high temperatures. The main contribution to the change of EIS comes from an increase in polarization resistance. Table 1 shows the polarization resistances of the LSC cell at various CO_2 partial pressures and different temperatures. The polarization resistance increases with increasing CO_2 partial pressure. At 500 °C, the polarization resistance is

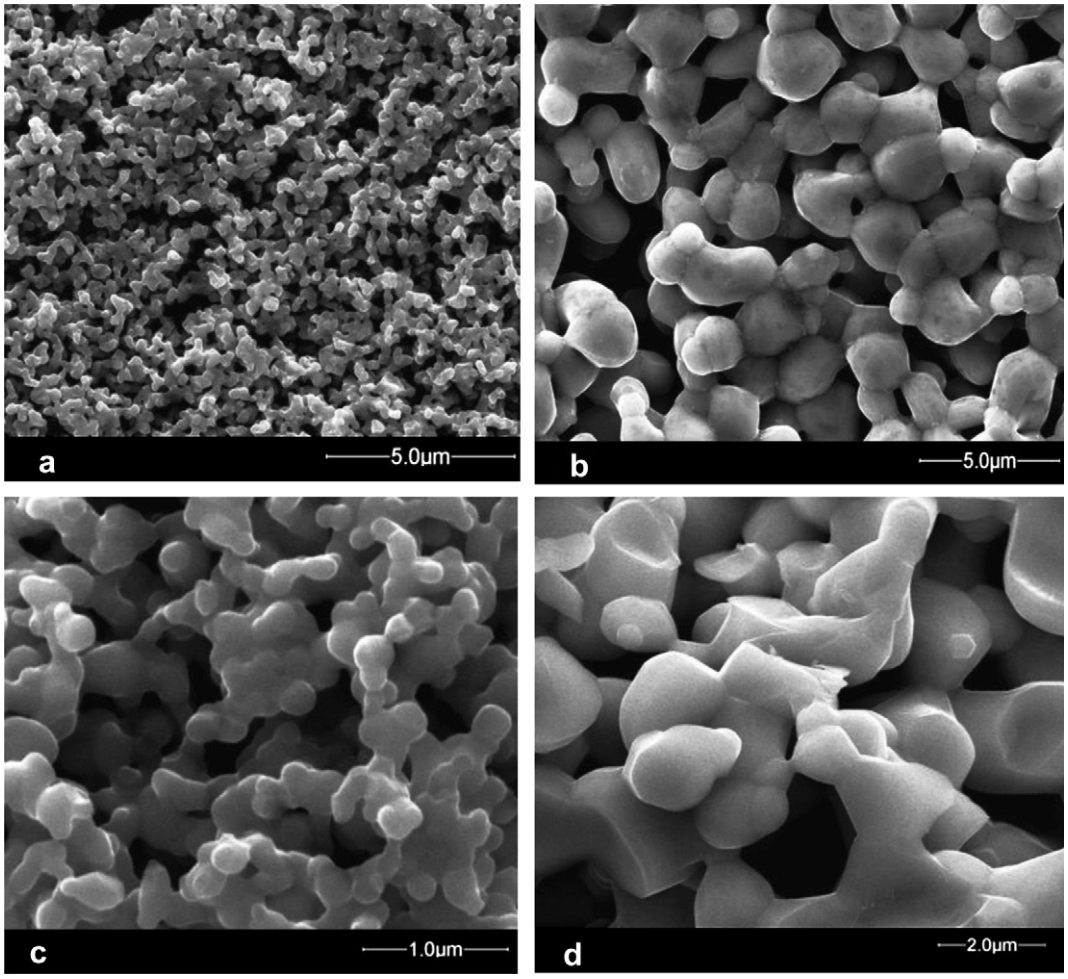

Fig. 1. Surface SEM images for (a) LSC cathode and (b) LSM cathode and cross sectional SEM images for (c) LSC cathode and (d) LSM cathode.

5.12 Ω cm^2 in O_2 flow, and increases to 5.74, 6.32, 6.66 and 7.03 Ω cm^2 at $P_{CO2} = 0.53$, 1.85, 2.99 and 4.68 kPa in oxidant. At the same CO_2 partial pressure, the increase in polarization resistance is more significant with decreasing temperature. At $P_{CO2} = 1.85$ kPa, the polarization resistance increases by 0.01 Ω cm^2 at 700 °C while it increases by 0.21 Ω cm^2 at 600 °C and 1.20 Ω cm^2 at 550 °C. The dependence of polarization resistance on temperature under O_2 flow is drawn with Arrenhius-Type relation. Two temperature ranges with different average activation energies are discriminated in the curve. The average activation energy is 123.6 kJ mol^{-1} below 670 °C and 27.2 kJ mol^{-1} above 670 °C, indicating the change of reaction mechanism at 670 °C. The low activation energy at high temperature indicates that the rate determining step can be gas diffusion from anode. Hydrogen dissociation and diffusion processes usually have so low activation energies [40,41]. At high temperatures, oxygen easily releases from LSC under cathodic polarization. The resulted oxygen vacancies greatly promote oxygen surface reaction on LSC [42,43]. That is to say, oxygen reduction on LSC cathode is no longer the rate limiting step above 670 °C. The apparent activation energy of cell reaction below 670 °C is in good agreement with that of oxygen surface exchange reported at interface LSC/LSGM and film LSC/YSZ [12,13,44]. Fig. 5 shows the effect of CO_2 partial pressure on apparent activation energy of the LSC cell at low temperatures. The apparent activation energy increases from 123.6 kJ mol^{-1} in pure O_2 to 131.1, 137.1, 139.1 and 140.9 kJ mol^{-1} at $P_{CO2} = 0.53$, 1.85, 2.99 and 4.68 kPa in oxidant.

The Bode plots in Fig. 4b show that the impedance of the LSC cell at least consists of three arcs, high frequency arc (summit frequency f_{summit} > ca.1000 Hz), intermediate frequency arc (f_{summit} ranging from ca.7.5–396 Hz) and low frequency arc (f_{summit} < ca. 2.5 Hz). This indicates that at least three rate determining steps are involved. At high temperatures of 700–800 °C, the low frequency impedance arc is dominant. The summit frequency and magnitude of low frequency arc almost do not vary with temperature, implying that the related activation energy is very low. The low frequency arc (f_{summit} < ca. 2.5 Hz) can arise from gas diffusion. The intermediate frequency arc is dominant at temperature range of 550–650 °C. The intermediate frequency arc significantly increases with decreasing temperature, and the summit frequency decreases with decreasing temperature, implying higher activation energy for the related reaction step. The intermediate frequency arc is correlated to the dissociative adsorption of oxygen according to the characteristic frequency [11–16,26,45]. The high frequency arc is related to the incorporation of oxygen ion into electrolyte. After introducing CO_2 to cathode, the change in impedance occurs mainly in the intermediate frequency region (f_{summit} ranging from ca.7.5–396 Hz), indicating that CO_2 impedes oxygen dissociative adsorption on LSC cathode.

Fig. 6 shows, in the form of Nyquist (Fig. 6a) and Bode (Fig. 6b) plots, the electrochemical impedance spectra of the LSM cell at various CO_2 partial pressures and temperatures. Similarly, the polarization resistance increases with increasing CO_2 partial

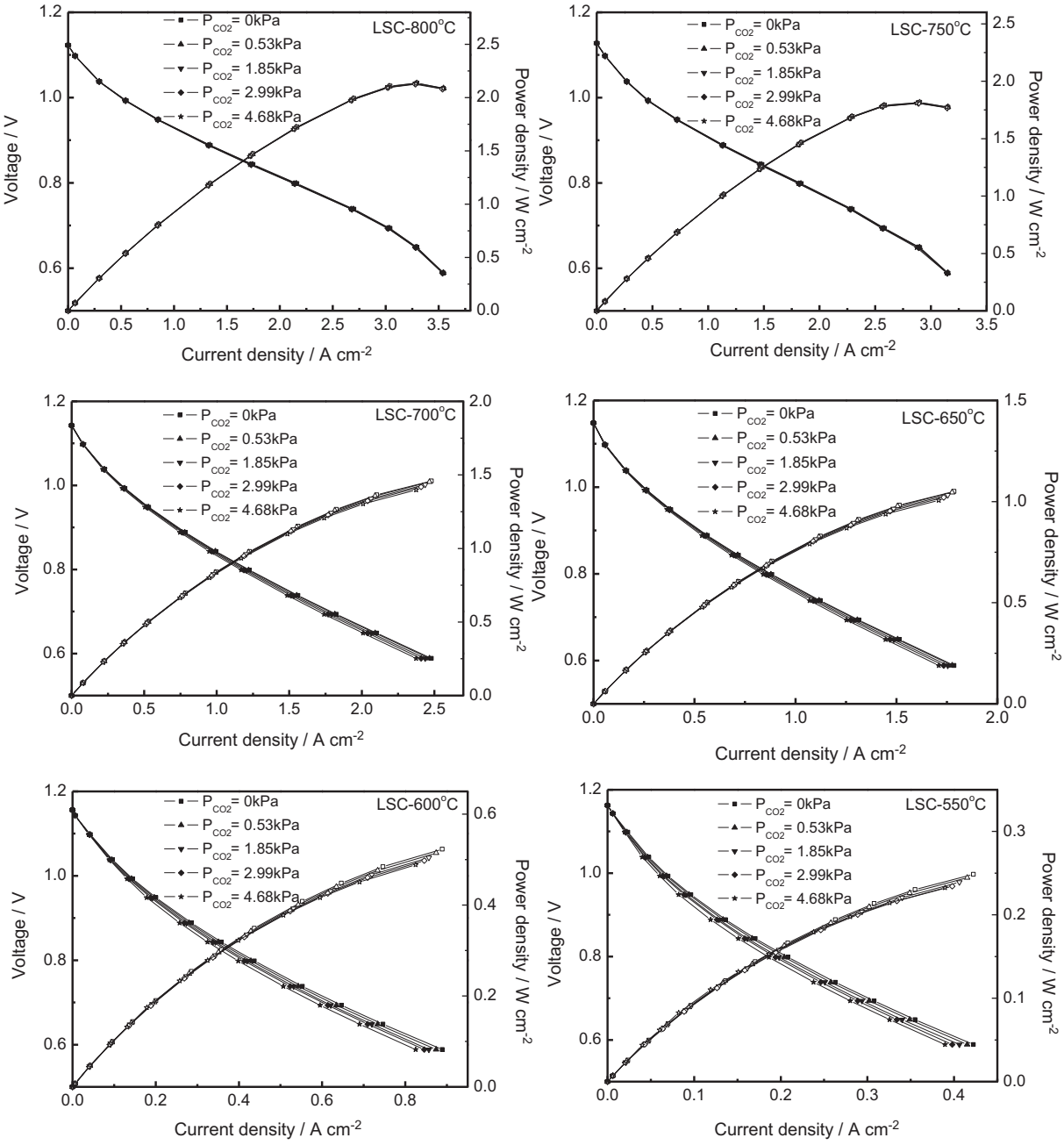

Fig. 2. Current density–voltage curves of the LSC cell at various CO_2 partial pressures from 550 °C to 800 °C.

pressure. Table 2 shows the polarization resistances at various CO_2 partial pressures and different temperatures on the LSM cell. At 700 °C, the polarization resistance is 2.94 Ω cm^2 under pure O_2 flow, and the polarization resistance increases to 2.97, 3.01, 3.07 and 3.14 Ω cm^2 at P_{CO2} = 0.53, 1.85, 2.99 and 4.68 kPa in oxidant. The increase in polarization resistance is more significant with decreasing temperature at the same CO_2 partial pressure. The variation in impedance is mainly assigned to the low frequency impedance arc with a summit frequency of ca. 2 Hz, which is associated with dissociation of adsorbed oxygen molecule or surface diffusion of O-species [46–48]. Thus, CO_2 impedes dissociation of adsorbed oxygen or surface diffusion of O-species on LSM. The dependence of the apparent activation energy on CO_2 partial pressure is depicted in Fig. 7. The apparent activation energy of the LSM cell is 80.6 kJ mol^{-1} when pure O_2 is used as oxidant. The apparent activation energy is 82.9, 83.6, 85.1 and 89.2 kJ mol^{-1} at P_{CO2} = 0.53, 1.85, 2.99 and 4.68 kPa in oxidant.

At a constant current density of 0.15 A cm^{-2}, the LSC cell voltage declines with increasing CO_2 partial pressure. The cell voltage decreases by 2.8, 8.8, 11.8 and 15.2 mV at 600 °C respectively when CO_2 partial pressure is 0.53, 1.85, 2.99 and 4.68 kPa in oxidant. At P_{CO2} = 1.85 kPa, the cell voltage decreases by 0.4, 0.6, 1.2, 3.9, 8.8 and 17.2 mV at 800, 750, 700, 650, 600 and 550 °C, respectively. The cell voltage can be written as equation (1).

$$V = E - iR_{ohm} - \eta_c(i) - \eta_a(i) \quad (1)$$

where E is electromotive force (EMF), R_{ohm} is ohmic resistance, η_c is cathodic overpotential, η_a is anodic overpotential. Even at P_{CO2} = 4.68 kPa, the variation in E caused by the change in oxygen

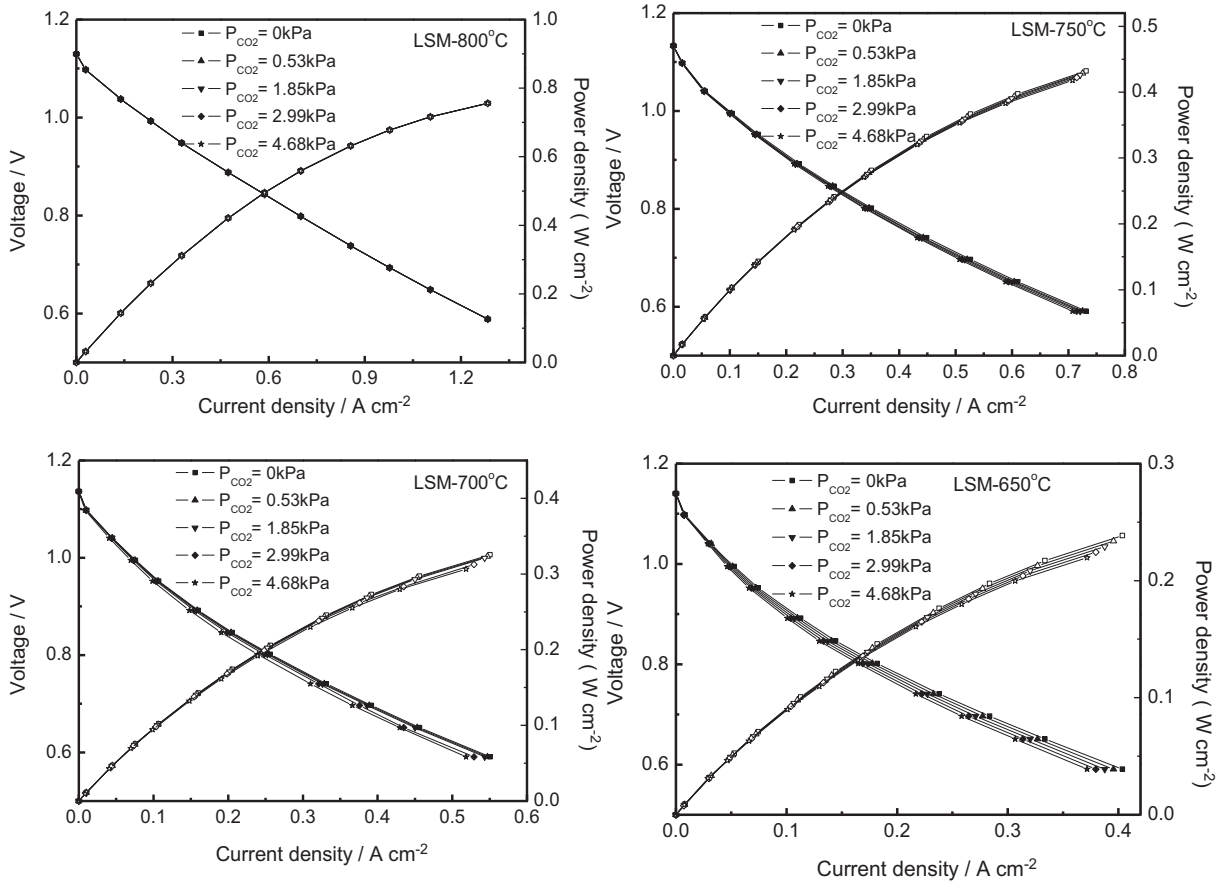

Fig. 3. Current density–voltage curves of the LSM cell at various CO_2 partial pressures from 650 °C to 800 °C.

partial pressure is 0.9 mV at 600 °C, which is far below the actual variation of 15.2 mV. The variation in E caused by the change in oxygen partial pressure is negligible for the cell voltage change. When low content of CO_2 is introduced into O_2 flow, the electromotive force (EMF) can be regarded as constant. Ohmic loss can also be regarded as constant due to fixed current density and constant R_{ohm}. Thus, the variation of cell voltage is considered as the variation of cathodic overpotential ($\Delta U = \Delta\eta_c$). A decrease in cell voltage means an increase in cathodic overpotential. The variation of cathodic interfacial resistance is evaluated using equation (2)

$$\Delta R_c = \Delta\eta_c / i \tag{2}$$

where $\Delta\eta_c$ is equal to ΔU, which is the change of cell voltage. i is current density (0.15 A cm^{-2}). Fig. 8 shows good linearity of Ln ($1/\Delta R_c$) versus reciprocal temperature for the LSC cathode in all temperature range. The results indicate that CO_2 affects the same oxygen reduction step whether at high temperatures or at low temperatures. This is consistent with the EIS results that CO_2 mainly influences oxygen dissociative adsorption. It can also be seen that the dependence of ΔR_c on temperature is stronger at low CO_2 partial pressures than that at high CO_2 partial pressures.

At a constant current density of 0.15 A cm^{-2}, the LSM cell voltage decreases with increasing CO_2 partial pressures. The voltage respectively decreases by 0.3, 0.9, 1.7 and 2.8 mV at 800 °C when CO_2 partial pressure is 0.53, 1.85, 2.99 and 4.68 kPa. At $P_{CO2} = 1.85$ kPa, the cell voltage decreases by 0.9 mV at 800 °C while it decreases by 2, 2.3 and 3.8 mV at 750, 700 and 650 °C, respectively. Similarly, good linearity of Ln ($1/\Delta R_c$) versus reciprocal temperature is observed on the LSM cell in Fig. 8, indicating that CO_2 affects the same oxygen reduction step. In contrast to the LSC cell, the dependence of ΔR_c on temperature for the LSM cell is stronger at high CO_2 partial pressures than that at low CO_2 partial pressures.

Oxygen reduction on cathode consists of three types of elementary reactions [6,8,49–51], surface reaction (1), surface and bulk diffusion (2) and incorporation into the electrolyte (3). Surface reaction involves adsorption of oxygen molecule (equation (3)), dissociative adsorption of oxygen molecule (equation (4)), dissociation of adsorbed oxygen molecule (equation (5)), ionization of oxygen atom (equation (6)), and transfer of oxygen ion from cathode surface into the bulk (equation (7)).

$$O_2(g) \rightarrow O_{2,ad} \tag{3}$$

$$O_2(g) \rightarrow 2O_{ad} \tag{4}$$

$$O_{2,ad} \rightarrow 2O_{ad} \tag{5}$$

$$O_{ad} \rightarrow O_{ad}^{2-} + 2h^{\bullet} \tag{6}$$

$$O_{ad}^{2-} + V_O^{\bullet\bullet} \rightarrow O_{O,cathode}^{x} \tag{7}$$

where $h^{\bullet}$ represents an electron hole. $V_O^{\bullet\bullet}$ is an oxygen vacancy. $O_{O,cathode}^{x}$ is a lattice oxygen. Assuming that (1) the steps involving the formation of adsorbed oxygen O_{ads} are slow, (2) oxygen activity on cathode surface varies approximately linearly with the concentration of adsorbed oxygen or the coverage of adsorbed

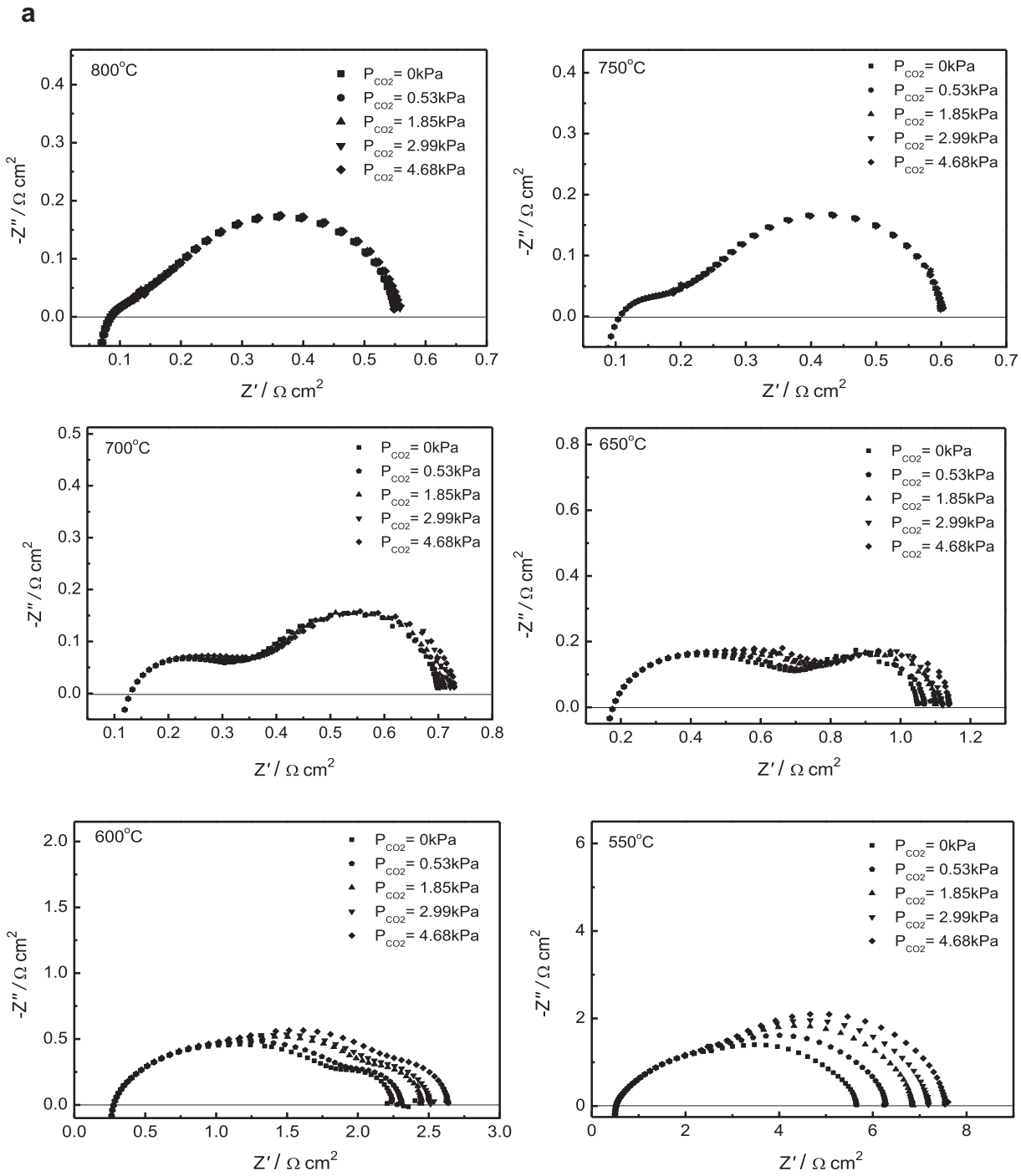

Fig. 4. Electrochemical impedance spectra of the LSC cell at various CO_2 partial pressures from 550 °C to 800 °C, Nyquist-plots (a), bode-plots (b).

oxygen, and (3) electrode potential lies on oxygen activity on cathode surface, the cathodic overpotential caused by surface reaction can be written as equation (8) [8,46].

$$\eta_{sr} = \frac{RT}{2F} \ln \frac{\theta_O^*}{\theta_O} \tag{8}$$

where θ_O^* is the coverage of adsorbed oxygen atom (O_{ads}) in equilibrium with the gas phase. Before introducing CO_2 to cathode, cathodic overpotential is expressed as equation (9). After introducing CO_2 to cathode, cathodic overpotential is expressed as equation (10). The variation in cathodic overpotential is written as equation (11).

$$\eta_{sr} = \frac{RT}{2F} \ln \frac{\theta_O^*}{\theta_O^{bef}} \tag{9}$$

$$\eta_{sr} = \frac{RT}{2F} \ln \frac{\theta_O^*}{\theta_O^{aft}} \tag{10}$$

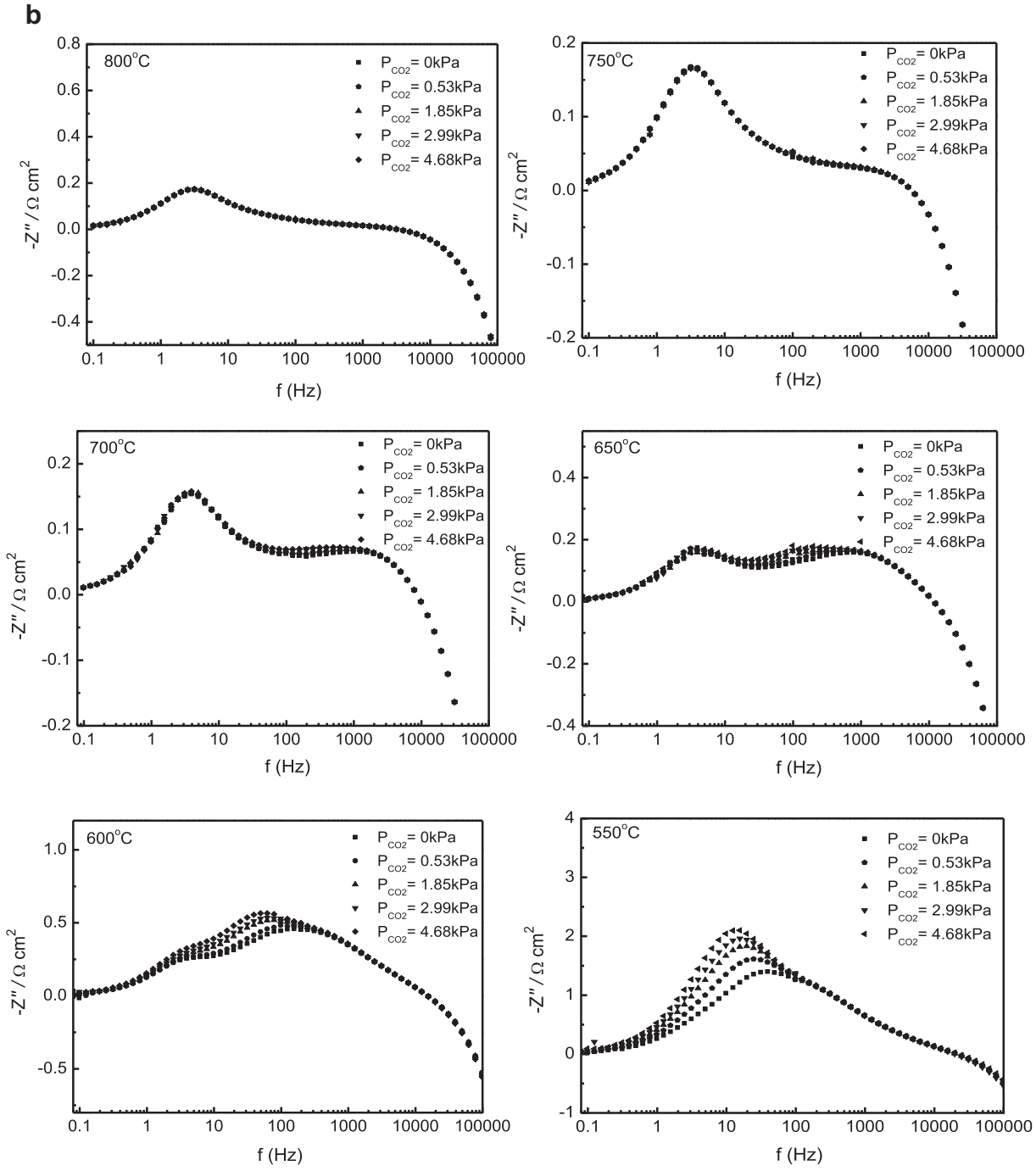

Fig. 4. (*continued*).

Table 1
Polarization resistances of the LSC cell at various CO_2 partial pressures from 550 °C to 800 °C.

Polarization resistance (Ω cm^2)						
CO_2 partial pressure (kPa)	550 °C	600 °C	650 °C	700 °C	750 °C	800 °C
0	5.12	1.97	0.87	0.57	0.49	0.46
0.53	5.74	2.03	0.89	0.57	0.49	0.46
1.85	6.32	2.18	0.92	0.58	0.50	0.47
2.99	6.66	2.23	0.95	0.60	0.50	0.47
4.68	7.03	2.36	0.96	0.60	0.51	0.47

$$\Delta\eta = \frac{RT}{2F}\ln\frac{\theta_O^{bef}}{\theta_O^{aft}} \tag{11}$$

Classic gas adsorption isotherms include Langmuir, Freundlich and Temkin equations. For surface where the adsorption heat is a function of coverage, a langmuir adsorption isotherm is not applicable. Here, Freundlich equation $\theta = kP^{1/n}$ and Temkin equations $\theta = a + b\ln(P)$ are proposed to describe the CO_2 chemisorption on cathodes. Where a, b, k and n are constants. Freundlich model assumes that adsorption heat logarithmically decreases with increasing surface coverage. Temkin model assumes that adsorption

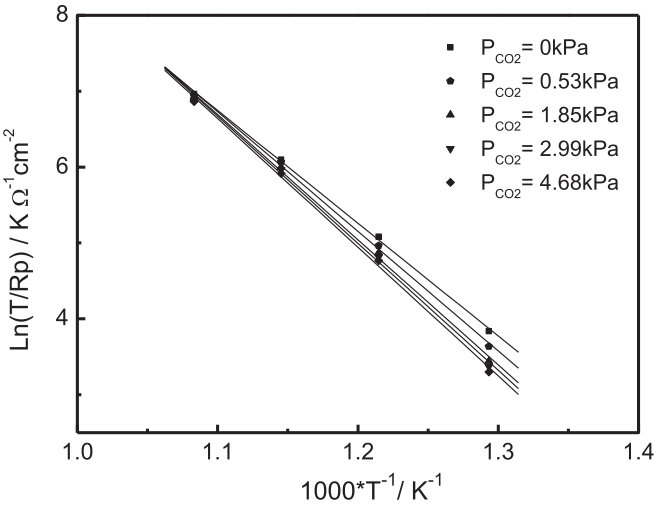

Fig. 5. Effects of CO_2 partial pressures on apparent active energies (Ea) of the LSC cell.

heat linearly decreases with increasing surface coverage. On the assumption that CO_2 competes with oxygen for same active sites, the coverage of adsorbed CO_2 can be evaluated on the basis of the variation in the coverage of oxygen. On the basis of evaluated CO_2 coverage and CO_2 partial pressure, the parameters a, b, k and n can be calculated. Then the average values of parameters are obtained. Thus, CO_2 adsorption equations (θ_{CO_2}) are determined. The variation in cathodic overpotential is recalculated using obtained CO_2 adsorption equations in order to check its validity on the basis of equation (12).

$$\Delta\eta = \frac{RT}{2F} \ln \frac{\theta_O^{bef}}{\theta_O^{bef} - \theta_{CO_2}} \tag{12}$$

Table 3 shows the linearization fitting parameters of CO_2 adsorption on LSC on the basis of Temkin equation and Freundlich equation. According to the linear correlation coefficients (R^2) values, Temkin model is adopted to describe CO_2 adsorption on LSC at low temperatures (550–650 °C), and Freundlich model is adopted to describe CO_2 adsorption on LSC at high temperatures (700–800 °C). The adsorption models show heterogeneous surface sites for CO_2 adsorption on LSC. Fig. 9 and Fig. 10 show a comparison of experimental data of $\Delta\eta_c$ and fitting data of $\Delta\eta_c$ on the basis of proposed CO_2 adsorption model at various temperatures. The good agreement between experimental data of $\Delta\eta_c$ and fitting data of $\Delta\eta_c$ indicates that the proposed CO_2 adsorption models on LSC at various temperatures are valid. The reason for that CO_2 adsorption obeys different models at different temperatures is related to the composition and structure changes in LSC as well as oxygen reduction mechanism. At low temperatures of 550–650 °C, oxygen dissociative adsorption on LSC cathode is a rate limiting step. CO_2

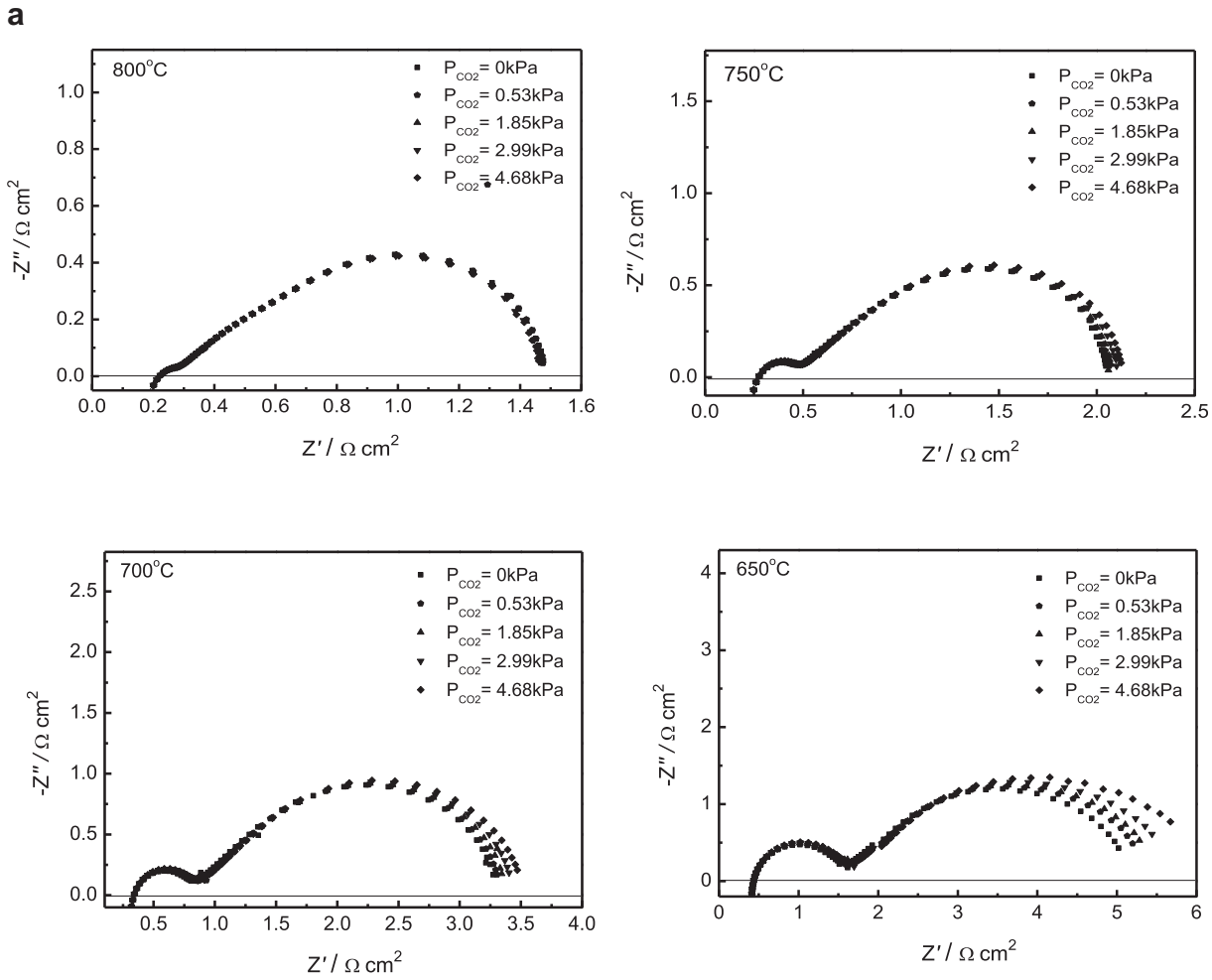

Fig. 6. Electrochemical impedance spectra of the LSM cell at various CO_2 partial pressures from 650 °C to 800 °C, Nyquist-plots (a), bode-plots (b).

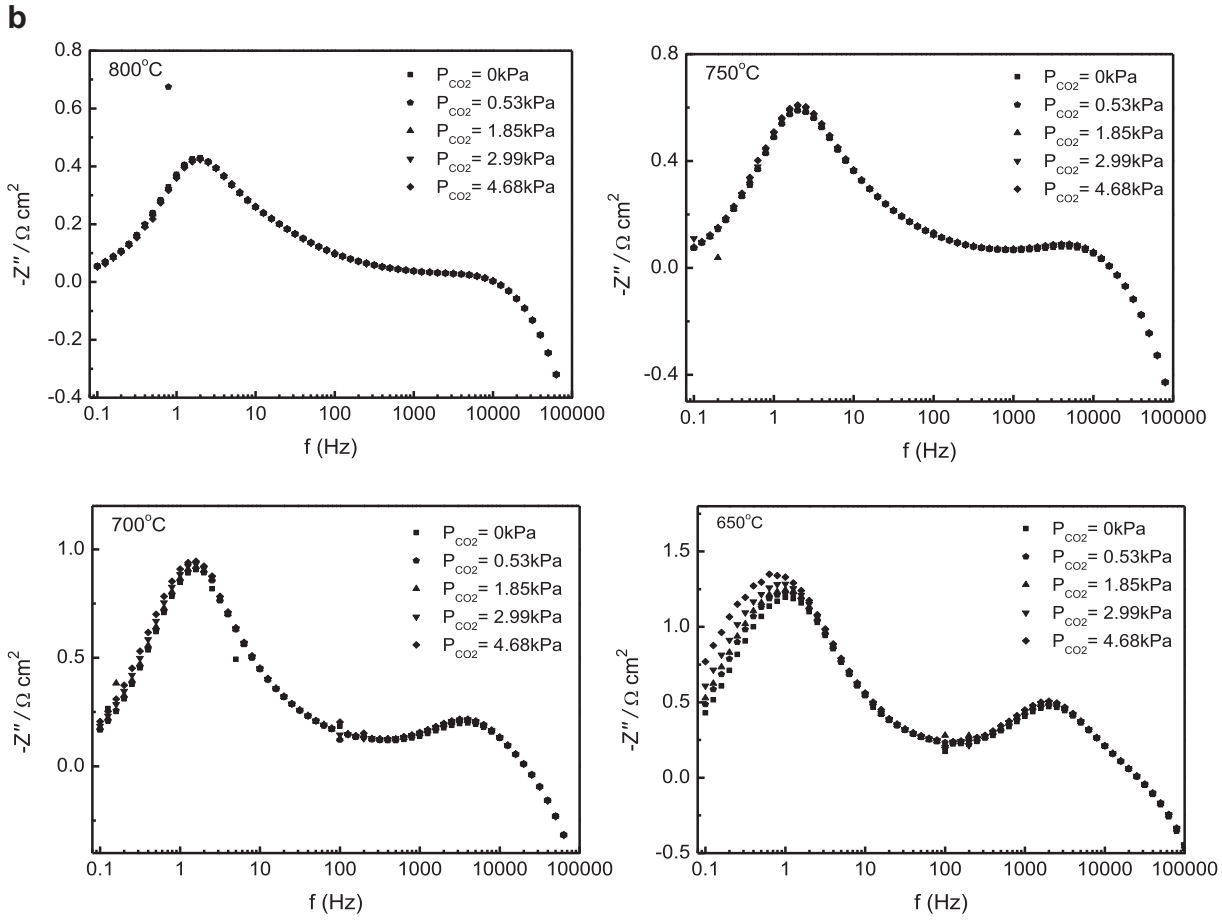

Fig. 6. (*continued*).

competes for ORR active sites with oxygen. The competitive adsorption of CO_2 with oxygen is favorable at low temperature. The dependence of CO_2 coverage on P_{CO2} is strong. CO_2 occupy greatly active sites as P_{CO2} increases even in low P_{CO2} range. A significant increase in cathodic overpotential with increasing P_{CO2} can be observed. CO_2 coverage approaches to maximum with further increasing P_{CO2}. The dependence of CO_2 coverage on CO_2 partial pressure becomes weak in high P_{CO2} range, which results in a small increase in cathodic overpotential with further increasing CO_2 partial pressure. At high temperatures of 700–800 °C, oxygen dissociative adsorption on LSC cathode becomes readily. As a result, the competitive adsorption of CO_2 with oxygen becomes relative weak. The dependence of CO_2 coverage on P_{CO2} is strong. CO_2 coverage gradually increases with increasing CO_2 partial pressure, which results in the increase in cathodic overpotential with increasing CO_2 partial pressure at high temperatures.

Table 4 shows that the linearization fitting parameters of CO_2 adsorption on LSM based on Temkin and Freundlich model. Freundlich model is adopted to describe CO_2 adsorption on LSM on the basis of R^2. Fig. 11 shows a comparison of experimental data and fitting data of $\Delta\eta_c$ on the basis of Freundlich model. The good agreement between experimental data and fitting data indicates that adopted CO_2 adsorption model for LSM cathode is valid. The EIS results reflect that oxygen dissociation or diffusion of O species is a slow process on LSM. The introduction of CO_2 can decrease oxygen available on the TPB and results in an increase in cathode

Table 2
Polarization resistances of the LSM cell at various CO_2 partial pressures from 650 °C to 800 °C.

Polarization resistance (Ω cm^2)				
CO_2 partial pressure (kPa)	650 °C	700 °C	750 °C	800 °C
0	4.60	2.94	1.78	1.26
0.53	4.82	2.97	1.80	1.26
1.85	4.90	3.01	1.80	1.27
2.99	5.12	3.07	1.84	1.28
4.68	5.47	3.14	1.86	1.27

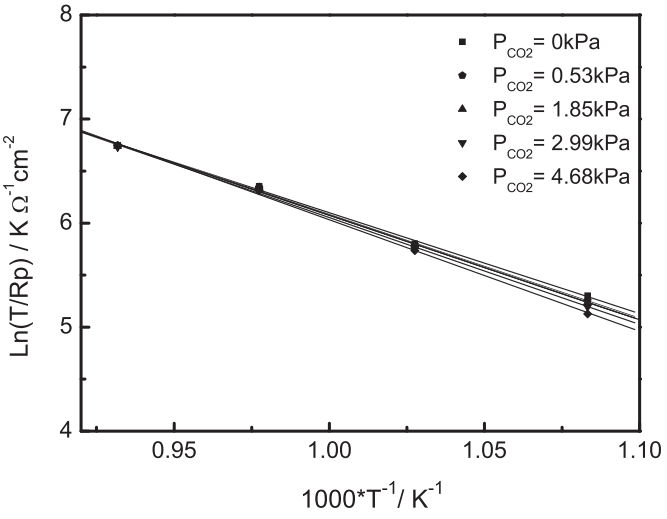

Fig. 7. Effects of CO_2 partial pressures on apparent active energies (Ea) of the LSM cell.

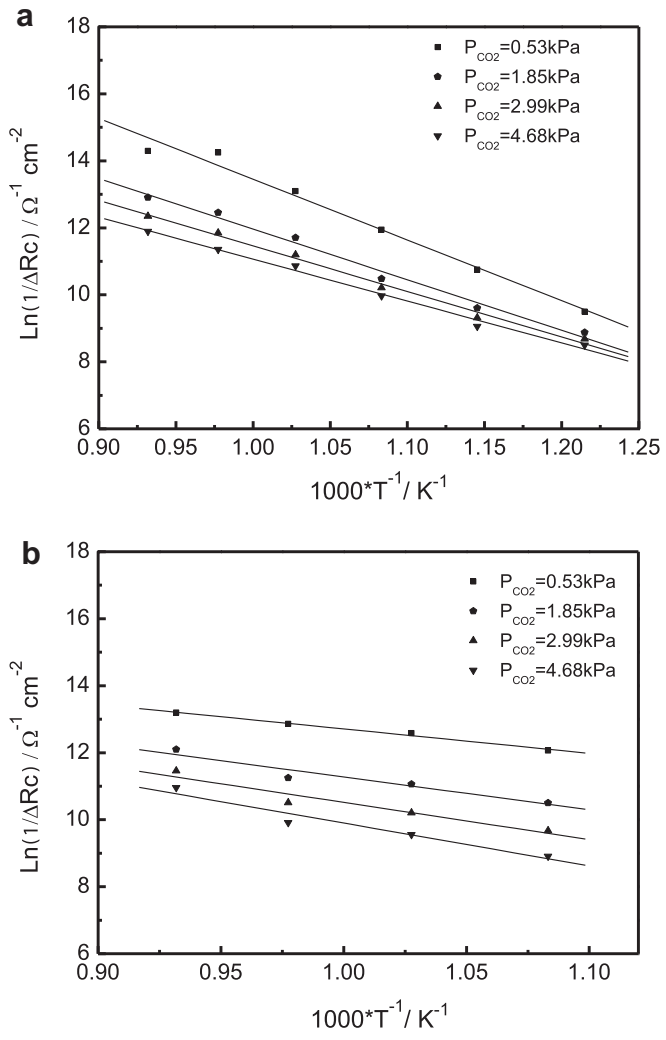

Fig. 8. Ln $(1/\Delta R_i)$ versus reciprocal temperature for the LSC cell (a) and the LSM cell (b) at various CO_2 partial pressures and temperatures. ΔR_c is the variation of cathodic interface resistance, which can be evaluated using equation $\Delta R_c = \Delta\eta_c/i$, in which $\Delta\eta_c$ is equal to the variation of cell voltage (ΔU), I is current density (0.15A cm^{-2}).

overpotential. CO_2 adsorption on LSM is relative weak as compared with CO_2 adsorption on Co-based perovskite [39]. The dependence of CO_2 coverage on CO_2 partial pressure is strong. CO_2 coverage gradually increases with increasing CO_2 partial pressure, which corresponds to the observation that the effect of CO_2 becomes serious with increasing CO_2 partial pressure. The present study of Freundlich model on CO_2 adsorption on LSM cathode is in agreement with a previous study on CO_2 adsorption on $LaMnO_{3+y}$ [56].

Oxygen reduction reaction on perovskite cathode depends on active B-site ions and oxygen vacancies. On one hand, the effect of

Table 3
Comparison of linearization parameter of CO_2 adsorption on LSC cathode at different temperatures based on Freundlich model $\theta = kP^{1/n}$ and Temkin model $\theta = a + b\ln(P)$.

Temperature (°C)	R^2	
	Freundlich model	Temkin model
550	0.9841	0.9993
600	0.9810	0.9974
650	0.9678	0.9981
700	0.9955	0.9462
750	0.9971	0.8937
800	0.9997	0.8986

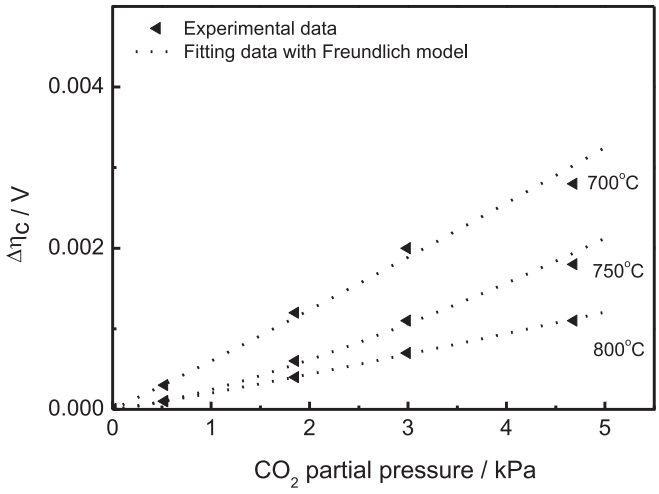

Fig. 9. Comparison of experimental data and fitting data of variation in cathodic overpotential ($\Delta\eta_c$) on the basis of Freundlich model for LSC cathode in temperature range of 700–800 °C.

electronic structure of B-site element on oxygen reduction reaction (ORR) of $LaBO_3$ perovskite has been investigated by theoretical and experimental studies [52–54]. ORR activity for perovskites is primarily related to the extent of hybridization of B–O bond and σ^*-orbital occupation. $LaMnO_3$ and $LaCoO_3$ display high ORR activity with an e_g-filling and the increased covalency between the metal 3d and oxygen 2p. When CO_2 adsorbs on a perovskite, both monodentate carbonates and bidentate carbonates are formed. Monodentate carbonate species are formed through C atom of CO_2 bonding with basic O^{2-} ion in perovskite. The basicity of O^{2-} ion depends on the electronegativity of cation. The electronegativity is 1.55, 1.88, 0.95 and 1.1 in the pauling scale for Mn, Co, Sr and La, respectively. The stability of monodentate carbonate bonding with A-site cation such as La and Sr is higher than that bonding with B-site cation such as Co and Mn. On the other hand, the amounts of oxygen vacancies in Mn-containing perovskite and Co-containing perovskite are different. Quantum mechanical analysis of $LaMO_3$ (M = Cr, Mn, Fe, Co) shows the difference in oxygen vacancy formation energies [55]. As compared with Mn-based perovskite, Co-based perovskite displays lower oxygen vacancy formation

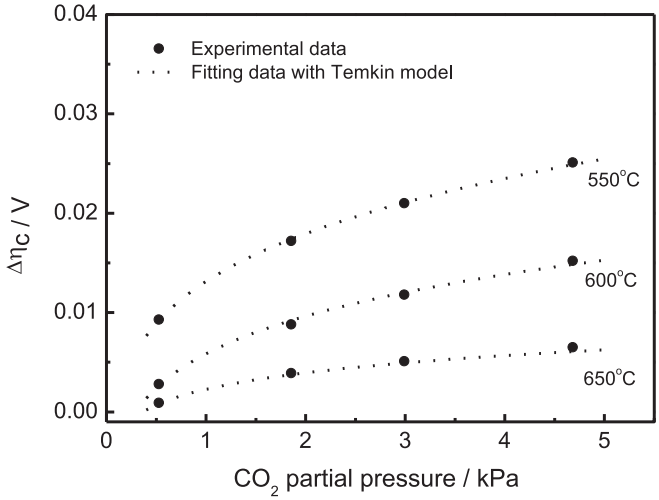

Fig. 10. Comparison of experimental data and fitting data of variation in cathodic overpotential ($\Delta\eta_c$) on the basis of Temkin model for LSC cathode in temperature range of 550–650 °C.

Table 4
Comparison of linearization parameter of CO_2 adsorption on LSM cathode at different temperature based on Freundlich model $\theta = kP^{1/n}$ and Temkin model $\theta = a + b\ln(P)$.

Temperature (°C)	R^2	
	Freundlich model	Temkin model
650	0.9961	0.8044
700	0.9952	0.8176
750	0.9991	0.8452
800	0.9920	0.8564

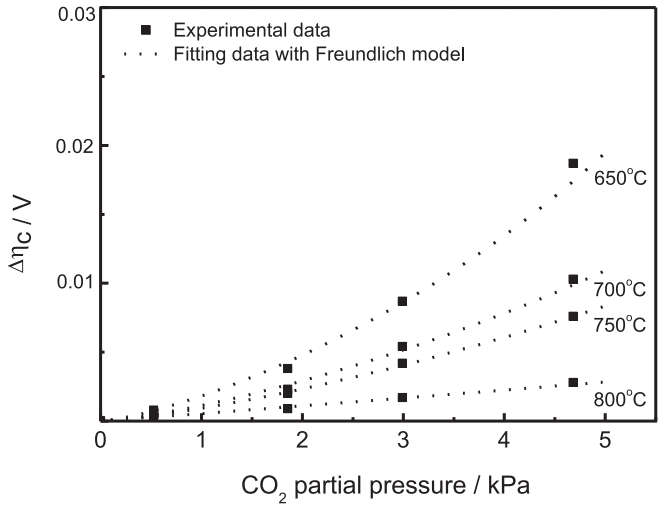

Fig. 11. Comparison of experimental data and fitting data of variation in cathodic overpotential ($\Delta\eta_c$) on the basis of Freundlich model for LSM cathode at temperature range of 650 °C–800 °C.

energy due to relative weaker Co–O bond strength and the ease of Co reduction. Mn-based perovskite displays oxygen excess non-stoichiometry while Co-based perovskite displays oxygen deficient nonstoichiometry. In our experiment, the absolute oxygen contents ($3 \pm \delta$) of initial $La_{0.6}Sr_{0.4}CoO_{3-\delta}$ (LSC) and $La_{0.8}Sr_{0.2}MnO_{3+\delta}$ (LSM) are 2.896 and 3.056, respectively. Under cathodic polarization or low oxygen partial pressure, oxygen vacancies can be further created. LSC displays a larger amount of oxygen vacancies than LSM. CO_2 is a slightly acid molecule. The adsorption of CO_2 on basic sites is strong. Bidentate carbonate species are formed through C atom of CO_2 bonding with basic O^{2-} ion in perovskite and O atom of CO_2 bonding with oxygen vacancy in perovskite [56,57]. The formation of oxygen vacancies increases the basicity of lattice oxygen and promotes CO_2 adsorption. Bidentate carbonates are more stable on LSC than on LSM.

4. Conclusions

The effects of CO_2 on $La_{0.6}Sr_{0.4}CoO_{3-\delta}$ (LSC) and $La_{0.8}Sr_{0.2}MnO_{3+\delta}$ (LSM) cathode were investigated. The presence of CO_2 in O_2 flow leads to a decrease in performance and an increase in polarization resistance. For the LSC cathode, the EIS results show a change in oxygen reduction mechanism on LSC at ca. 670 °C. Gas diffusion in anode can be the rate limiting step at high temperatures, whereas oxygen dissociative adsorption is the rate liming step at low temperatures. CO_2 impedes oxygen dissociative adsorption on LSC at all temperatures. CO_2 adsorption on LSC obeys Temkin model at low temperatures (550–650 °C) and Freundlich model at high temperatures (700–800 °C). Different CO_2 adsorption behaviors are ascribed to the change in LSC structure and the change in oxygen reduction mechanism. For the LSM cathode, oxygen reduction mechanism does not change in all the temperature range (650–800 °C). CO_2 inhibits oxygen dissociation adsorption and diffusion of oxygen species on LSM. CO_2 adsorption on LSM obeys Freundlich model in all the temperature range (650–800 °C). The differences in the effects and affecting mechanisms of CO_2 on LSM and LSC are related to their differences in composition and structure.

Acknowledgments

This work is supported by the Ministry of Science and Technology of China (No. 2010CB732302 and 2011AA050704) and National Natural Science Foundation of China (No.21076209, 20876156 and 20803073)

References

[1] I. Yasuda, K. Ogasawara, M. Hishinuma, T. Kawada, M. Dokiya, Solid State Ionics 86–88 (1996) 1197–1201.
[2] Y.D. Zhen, S.P. Jiang, J. Electrochem. Soc. 153 (2006) A2245–A2254.
[3] J. Mizusaki, N. Mori, H. Takai, Y. Yonemura, H. Minamiue, H. Tagawa, M. Dokiya, H. Inaba, K. Naraya, T. Sasamoto, T. Hashimoto, Solid State Ionics 129 (2000) 163–177.
[4] J. Mizusaki, H. Tagawa, K. Naraya, T. Sasamoto, Solid State Ionics 49 (1991) 111–118.
[5] J. Mizusaki, H. Tagawa, J. Electrochem. Soc. 138 (1991) 1867–1873.
[6] E. Ivers-Tiffée, A. Weber, H. Schichlein, Handbook of Fuel Cells-Fundamentals, Technology and Applications.
[7] H. Kamata, A. Hosaka, J. Mizusaki, H. Tagawa, Solid State Ionics 106 (1998) 237–245.
[8] J.V. Herle, A.J. McEvoy, K.R. Thampi, Electrochim. Acta 41 (1996) 1447–1454.
[9] A. Hammouche, E. Siebert, M. Kleitz, J. Electrochem. Soc. 138 (1991) 1212–1216.
[10] E. Siebert, A. Hammouche, M. Kleitz, Electrochim. Acta 40 (1995) 1741–1753.
[11] A. Weber, E. Ivers-Tiffée, J. Power Sources 127 (2004) 273–283.
[12] B.J. Januschewsky, M. Ahrens, A. Opitz, F. Kubel, J. Fleig, Adv. Funct. Mater. 19 (2009) 3151–3156.
[13] A.N. Petrov, O.F. Kononchuk, A.V. Andreev, V.A. Cherepanov, P. Kofstad, Solid State Ionics 80 (1995) 189–199.
[14] Y.X. Lu, C. Kreller, S.B. Adler, J. Electrochem. Soc. 156 (2009) B513–B525.
[15] S.B. Adler, Solid State Ionics 111 (1998) 125–134.
[16] T. Horita, K. Yamaji, N. Sakai, H. Yokokawa, A. Weber, E. Ivers-Tiffée, J. Electrochem. Soc. 148 (2001) A456–A462.
[17] M. Gödickemeier, K. Sasaki, L.J. Gauckler, I. Riess, Solid State Ionics 86-88 (1996) 691–701.
[18] M. Gödickemeier, K. Sasaki, L.J. Gauckler, J. Electrochem. Soc. 144 (1997) 1635–1646.
[19] S.B. Adler, Chem. Rev. 104 (2004) 4791–4843.
[20] H. Yokokawa, K. Yamaji, M.E. Brito, H. Kishimoto, T. Horita, J. Power Sources 196 (2011) 7070–7075.
[21] H. Yokokawa, H.Y. Tu, B. Iwanschitz, A. Maic, J. Power Sources 182 (2008) 400–412.
[22] J. Nielsen, M. Mogensen, Solid State Ionics 189 (2011) 74–81.
[23] F.F. Wang, K. Yamaji, D.-H. Cho, T. Shimonosono, H. Kishimoto, M.E. Brito, T. Horita, H. Yokokawa, J. Electrochem. Soc. 158 (2011) B1391–B1397.
[24] Y.P. Xiong, K. Yamaji, T. Horita, H. Yokokawa, J. Akikusa, H. Eto, T. Inagaki, J. Electrochem. Soc. 156 (2009) B588–B592.
[25] R.R. Liu, S.H. Kim, Y. Shiratori, T. Oshima, K. Ito, K. Sasaki, ECS Trans. 25 (2009) 2859–2866.
[26] P. Hjalmarsson, M. Sogaard, M. Mogensen, Solid State Ionics 179 (2008) 1422–1426.
[27] J.H. Joo, R. Merkle, J. Maier, J. Power Sources 196 (2011) 7495–7499.
[28] J. Nielsen, A. Hagen, Y.L. Liu, Solid State Ionics 181 (2010) 517–524.
[29] A. Hagen, K. Neufeld, Y.L. Liu, J. Electrochem. Soc. 157 (2010) B1343–B1348.
[30] C. Knöfel, M. Chen, M. Mogensen, Fuel Cells 11 (2011) 669–677.
[31] A.Y. Yan, M.J. Cheng, Y.L. Dong, W.S. Yang, V. Maragou, S.Q. Song, P. Tsiakaras, Appl. Catal. B-Environ. 66 (2006) 64–71.
[32] A.Y. Yan, V. Maragou, A. Arico, M.J. Cheng, P. Tsiakaras, Appl. Catal. B-Environ. 76 (2007) 320–327.
[33] A.Y. Yan, B. Liu, Y.L. Dong, Z.J. Tian, D.Z. Wang, M.J. Cheng, Appl. Catal. B-Environ. 80 (2008) 24–31.
[34] E. Bucher, A. Egger, G.B. Caraman, W. Sitte, J. Electrochem. Soc. 155 (2008) B1218–B1224.
[35] L.G. Tejuca, A.T. Bell, Appl. Surf. Sci. 37 (1989) 353–366.
[36] L.G. Tejuca, A.T. Bell, Appl. Surf. Sci. 31 (1988) 301–316.
[37] J.M.D. Tascon, L.G. Tejuca, J.Chem.Soc., Faraday Trans.1 77 (1981) 591–602.
[38] V.C. Corberan, L.G. Tejuca, A.T. Bell, J. Mater. Sci. 24 (1989) 4437–4442.
[39] M.A. Pena, J.L.G. Fierro, Chem. Rev. 101 (2001) 1981–2017.
[40] S.P. Jiang, S.P.S. Badwal, Solid State Ionics 123 (1999) 204–224.
[41] X.-D. Zhou, L.R. Pederson, J.W. Templeton, J.W. Stevenson, J. Electrochem. Soc. 157 (2) (2010) B220–B227.

[42] E. Bucher, W. Jantscher, A. Benisek, W. Sitte, W. Preis, I. Rom, F. Hofer, Solid State Ionics 141–142 (2001) 375–380.
[43] L.-W. Tai, M.M. Nasrallah, H.U. Anderson, D.M. Sparlin, S.R. Sehlin, Solid State Ionics 76 (1995) 259–271.
[44] Y.L. Yang, C.L. Chen, C.W. Chu, A.J. Jacobson, J. Electrochem. Soc. 147 (2000) 4001–4007.
[45] V. Ch Kournoutis, F. Tietz, S. Bebelis, Fuel Cells 9 (2009) 852–860.
[46] S.P. Jiang, Solid State Ionics 146 (2002) 1–22.
[47] M.J. Jorgensen, M. Mogensen, J. Electrochem. Soc. 145 (2001) A433–A442.
[48] S. Primdahl, M. Mogensen, J. Electrochem. Soc. 145 (1998) 2431–2438.
[49] C.C. Kan, H.H. Kan, F.M. Van Assche IV, E.N. Armstrong, E.D. Wachsmana, J. Electrochem. Soc. 155 (2008) B985–B993.
[50] C.C. Kan, E.D. Wachsmana, Solid State Ionics 181 (2010) 338–347.
[51] Y. Jiang, S.Z. Wang, Y.H. Zhang, J.W. Yan, W.Z. Li, Solid State Ionics 110 (1998) 111–119.
[52] J. Suntivich, H.A. Gasteiger, N. Yabuuch, H. Nakanish, J.B. Goodenough, Y.S. -Horn, Nat. Chem. 3 (2011) 546–550.
[53] J.Q. Yan, J.S. Zhou, J.B. Goodenough, Phys. Rev. B 70 (2004) 014402.
[54] F.J. Morin, T. Wolfram, Phys. Rev. Lett. 30 (1973) 1214–1217.
[55] M. Pavone, A.M. Ritzmann, E.A. Carter, Energy Environ. Sci. 4 (2011) 4933–4937.
[56] R. Hammami, H. Batis, C. Minot, Surf. Sci. 603 (2009) 3057–3067.
[57] R. Hammami, A. Dhouib, S. Fernandez, C. Minot, Catal. Today 139 (2008) 227–233.